

Light-induced scattering of femtosecond laser pulses in iron-doped lithium niobate crystals

Johanna Bückers, Dominik Maxein,* Daniel Haertle, and Karsten Buse

Institute of Physics, University of Bonn, Wegelerstr. 8, D-53115 Bonn, Germany

**Corresponding author: maxein@uni-bonn.de*

Received December 2, 2008; revised March 16, 2009; accepted March 16, 2009;
posted March 18, 2009 (Doc. ID 104691); published April 16, 2009

Self-amplification of weak scattered coherent light waves in photorefractive crystals leads to losses, known as light-induced scattering or holographic scattering. We find with 532 nm light that it is reduced in $\text{LiNbO}_3:\text{Fe}$ for femtosecond laser pulses as compared to cw laser light. Light-induced scattering of pulses is completely absent in samples with sufficiently small Fe^{2+} content, in contrast to the scattering of cw light. Additional differences include a slower buildup time, a weaker Bragg selectivity, and a narrower angular distribution of the scattered light for pulsed illumination. The differences can be attributed mainly to the smaller temporal coherence of pulses. © 2009 Optical Society of America

OCIS codes: 160.5320, 160.3730, 120.5820.

1. INTRODUCTION

Laser light traversing a photorefractive medium is usually subject to light-induced scattering (LIS), also referred to as holographic scattering or photo-induced light scattering (PILS) [1,2]. This arises from parasitic gratings created from the interference of the laser beam with its own scattered light, which is intensified through photorefractive two-wave mixing at the expense of the original beam. The resulting destruction of the beam shape hinders photonic applications like holographic spectral filtering [3–6], optical image processing [7,8], and holographic diffractive beam shaping [9]. However, light-induced scattering can also be useful for material characterization [10,11].

Another beam degradation effect, the so-called “optical damage” [12], is a self-refracting effect originating from light-induced refractive-index changes. In contrast, light-induced scattering is based on self-diffraction [13], which requires interference and thus occurs for coherent light only.

For all applications utilizing femtosecond (fs) pulses and nonlinear crystals like lithium niobate (LiNbO_3), it will be relevant to explore how strong holographic scattering is. Although a first study of such effects exist [14], we concentrate here on a thorough comparison of holographic scattering induced by cw and fs visible light, revealing a strong influence of the kind of illumination on the scattering.

2. EXPERIMENTAL SETUP

Fs pulses of 532 nm wavelength are generated by optical parametrical amplification and sum frequency generation using a CPA2010 laser (from Clark MXR Inc.) feeding a TOPAS system (from Light Conversion Inc.). The resulting pulses have about 150 fs FWHM duration and a repetition rate of 1 kHz. Alternatively, cw light of 532 nm

originating from a frequency-doubled Nd:YAG laser is employed. For the sake of simplicity, we will speak of power and intensity also for the pulsed beam, where this corresponds to the pulse energy times the laser repetition rate and the average intensity over many pulses, respectively.

The laser light is sent through a zero-order wave plate and a Glan laser polarizer. While the latter defines the light polarization, the former can be used to vary the beam power. The crystal is illuminated perpendicular to the front surface and its c axis. About 5 cm behind the crystal, there is a 2.2 mm wide rectangular diaphragm. It allows the unchanged main beam to pass completely through its center but blocks light scattered out of its original direction. The light coming through the diaphragm is collimated with a lens onto a silicon photodiode measuring the power $P(t)$ of the transmitted beam as a function of time t . The relative transmission is defined as $T(t) = P(t)/P_{\text{max}}$, where P_{max} is the maximum power measured.

The samples are congruent lithium niobate crystals doped with iron ($\text{LiNbO}_3:\text{Fe}$). We examined three series of crystals cut from three boules with different iron dopant concentrations: DT1 ($7 \times 10^{24} \text{ m}^{-3}$), EQ2 ($20 \times 10^{24} \text{ m}^{-3}$), and DT2 ($56 \times 10^{24} \text{ m}^{-3}$). As-grown crystals have been used as well as oxidized and reduced samples. To oxidize and reduce the crystals, thermal annealing was employed in oxygen and in moderate vacuum, respectively [15]. The concentration $c_{\text{Fe}^{2+}}$ of iron in the valence state 2+ is measured by absorption spectroscopy using the relation $c_{\text{Fe}^{2+}} = 2.16 \times 10^{21} \text{ m}^{-1} \alpha_{477,0}$ [16], where $\alpha_{477,0}$ is the absorption constant at 477 nm for ordinary light polarization.

The crystals have the dimensions $0.5 \times (0.8\text{--}1.0) \times 1 \text{ mm}^3$ along x , y , and z axes, respectively, where z is parallel to the c axis of the crystal. The light propagates along x and is polarized parallel to z (extraordinary polarization). The beam diameter is at least 1.5 mm FWHM, ensuring homogeneous illumination of the crystal along

the z axis. Unless noted otherwise, the c faces of the crystals are short-circuited with conductive silver paint to prevent a macroscopic charge buildup due to the bulk photovoltaic effect at these faces. The samples are mounted on a rotation stage and can be turned around the y axis for measurements of the angular selectivity of the light-induced scattering and for off-Bragg erasure.

3. RESULTS

A. Temporal Evolution and General Observations

A selection of measurements from two typical series is shown in Fig. 1. Immediately after beginning with the illumination, the transmission T starts to decrease until it saturates at a value T_{sat} . Saturation is reached faster at higher intensities. The remaining transmission T_{sat} varies from crystal to crystal but for the same crystal almost the same T_{sat} is reached regardless of the intensity. There is a slight trend towards less scattering for weaker intensities, but only for the weakest intensity in each series, T_{sat} deviates significantly from the other values while still being of the same order of magnitude. It can be seen that the scattering builds up faster and is more strongly pronounced for cw light than for the fs pulses.

The scattering properties of the crystal persist in the dark, at least on the timescale of minutes. When the laser beam is blocked for a short time, it experiences the same losses immediately before and after the interruption. However, the effect can be completely annihilated by illuminating the sample with white light or alternatively with the writing light under permanently varying angles. This clearly indicates that the observed scattering is of photorefractive origin.

To rule out macroscopic refractive index changes, like the formation of a defocusing gradient-index lens, we checked crystals in an interferometer after cw and pulsed illumination. With these measurements, no deviations in the illuminated regions could be observed. Therefore, on a scale of about 0.1 mm, long-range index changes larger than 3×10^{-4} can be excluded, and microscopic index pat-

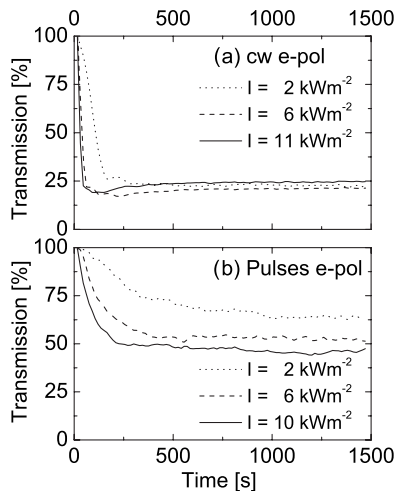


Fig. 1. Writing curves. Transmission through an as-grown DT2 crystal with different intensities for extraordinarily polarized (a) cw light and (b) pulses, respectively. The average intensities for the cw and pulse measurements are in the same range.

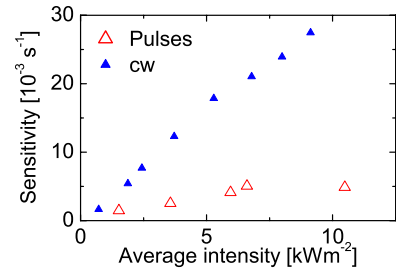


Fig. 2. (Color online) Sensitivity S in an as-grown DT2 crystal as a function of the average intensity for extraordinarily polarized cw and pulsed light.

terns must play a role. Furthermore, the pulse-illuminated crystal becomes iridescent. When looking through it against white light under small angles, light of different colors is diffracted into the eye, depending on the orientation of the crystal regarding the incoming white light. This also indicates the existence of gratings in the sample.

All results described lead to the conclusion that the effect observed is indeed light-induced scattering at parasitic, photorefractive gratings. To describe its initial buildup speed, the sensitivity S is used:

$$S = \left. \frac{\partial}{\partial t} \sqrt{\eta} \right|_{t=0}.$$

Here, the loss efficiency $\eta(t) = 1 - T(t)$ describes how efficiently light is deflected out of the laser beam. In practice, S is determined by a linear fit to the data from the beginning to the time when the effect has reached 60% of its maximum value. For the measurements in an as-grown DT2 sample, this sensitivity is shown in Fig. 2. We find that S depends approximately linearly on the intensity. It is larger for cw light than for pulses, i.e., saturation is reached faster for cw light than for pulses of the same average intensity.

B. Dependence on the Fe^{2+} Content

The strength of light-induced scattering is shown in Fig. 3 for cw and pulsed illumination for all samples available. Up to an Fe^{2+} concentration of about $1 \times 10^{24} \text{ m}^{-3}$, none of the crystals shows light-induced scattering upon pulse ex-

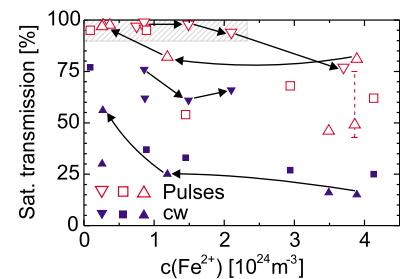


Fig. 3. (Color online) Dependence of the saturated transmission T_{sat} on the Fe^{2+} concentration. Open symbols represent pulse measurements, while closed symbols indicate cw light measurements. The different shapes of the symbols correspond to the total Fe concentration of the respective sample (Δ , $56 \times 10^{24} \text{ m}^{-3}$; \square , $20 \times 10^{24} \text{ m}^{-3}$; ∇ , $7 \times 10^{24} \text{ m}^{-3}$). Arrows connect measurements using the same sample before and after a thermal treatment. The measurements in the shaded area reveal no light-induced scattering.

posure. Above this concentration, scattering occurs in some samples. The shaded area in Fig. 3 marks all measurements where scattering is absent. For cw illumination, however, all crystals show light-induced scattering, which is always much stronger than for fs pulses.

To check whether indeed the Fe^{2+} concentration is the relevant parameter, we subject two crystals to consecutive thermal treatments and look for the light-induced scattering before and after the treatments. These measurement points are connected with arrows in Fig. 3. The DT1 crystal (∇) doesn't show the effect with pulses initially and after the first and second reduction treatment. However, after further annealing, the light-induced scattering becomes clearly visible. The DT2 crystal (Δ) contains more Fe^{2+} in the as-grown state than the sample DT1 because of the higher Fe content. Here, light-induced scattering exists in the as-grown state and after one oxidation treatment, but it vanishes after the second, stronger oxidation. Thus we find that for each crystal series DT1, EQ2, and DT2, there is a certain Fe^{2+} concentration below which the effect is not observed; crystals above this concentration are always affected. This limit shifts to higher Fe^{2+} values for lower Fe content.

C. Bragg Selectivity

To test the angular selectivity of the light-induced scattering, we rotate the crystals around the y axis, after the saturation is reached and look for changes in the transmission. For this measurement, the laser beam is attenuated to reduce the amount of erasure. The results are shown in Fig. 4. Both cw and pulse scattering shows a pronounced angular selectivity. It is considerably sharper when using cw light than when using femtosecond pulses. Within the measurement accuracy, the minimum transmission occurs in the cw case at the same angle as the foregoing illumination, i.e., at 0° . For pulses, the minimum is shifted. It is reached when rotating the crystal about 0.5° away from the original exposure direction.

D. Scattering Directions

In order to see the deflected light, we remove the silver paint from the side faces of the crystals; these measurements show the same strength of the light-induced scattering. The deviated light manifests itself quite differently for pulses and cw light. If a loss is observed for pulses, scattering lobes will build up alongside the main beam in the plane of the c axis and the beam propagation; see, e.g., Fig. 5. For cw illumination, the scattering observed behind the crystal is much fainter and broader.

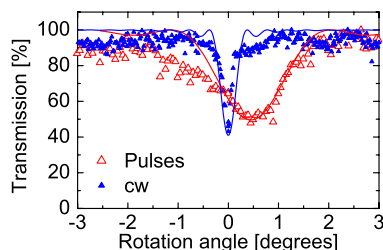


Fig. 4. (Color online) Angular selectivities of light-induced scattering for cw light and for pulses with comparable average intensities for an as-grown sample DT2. The curves are calculated based on a simple model explained in Section 4.

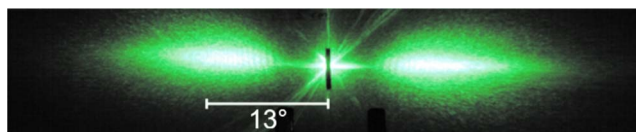


Fig. 5. (Color online) Photo of scattered fs pulsed light on a screen 27 cm behind the crystal.

this case, most of the light missing from the transmitted beam leaves the crystal through the unpolished c face, i.e., the side of the crystal. Necessarily, most of the cw light must be scattered at least under the angle of total internal reflection inside the crystal. However, by focusing the cw beam to a FWHM width of $200\ \mu\text{m}$, i.e., smaller than the crystal width, and attenuating it to similar intensities as above, one yields a scattering pattern similar to those observed with fs pulses.

4. DISCUSSION

A. Origin of the Scattering

For cw light as well as for pulses, the general reason for the observed losses is light-induced scattering at parasitic gratings. The optical erasability of the effect, the lack of macroscopic index changes, and the appearance of the pulse-illuminated crystal in white light as well as the strong angular dependence of the light deflection point to diffraction from photorefractive gratings as the reason for the loss of light.

In a photorefractive crystal, a multitude of light-induced scattering processes is possible [17]. As shown in [18] for a small signal beam and light-induced scattering, the different processes compete against each other for amplification by the pump beam. In our experiments, the fs light is scattered in the forward direction and looks similar to scattering lobes previously observed in LiNbO_3 [19]. When the crystal is illuminated with cw light homogeneously along the c axis, the light leaves the crystal at the side faces. Such scattering has been reported by Liu *et al.* as the light-climbing effect [20]. Obviously, other scattering processes prevail for fs pulses than for cw light.

It is beyond the scope of this work to decide which processes precisely dominate for pulses and cw light, respectively. However, we would like to understand which properties are in general responsible for the observed differences between scattering induced by cw light and pulses. One may argue that the much higher peak intensity of the fs pulses plays a role. This would lead to an increase of nonlinear excitations. However, as we can see from Fig. 2, the sensitivity for pulses is smaller than for cw light, and it increases roughly linearly with the average intensity. Both facts suggest that additional nonlinear excitations by the pulses can be neglected. For fs pulses of longer wavelengths, nonlinear excitations might play an important role, as Wu *et al.* conclude in [14] for near-IR light.

B. Impact of the Different Coherence Lengths

In contrast to cw light, pulses have a limited extension in the direction of propagation, which is about $(c/n) \times 200\ \text{fs} \approx 25\ \mu\text{m}$ in our experiments. As illustrated in Fig. 6, this leads to an important limitation. Not every-

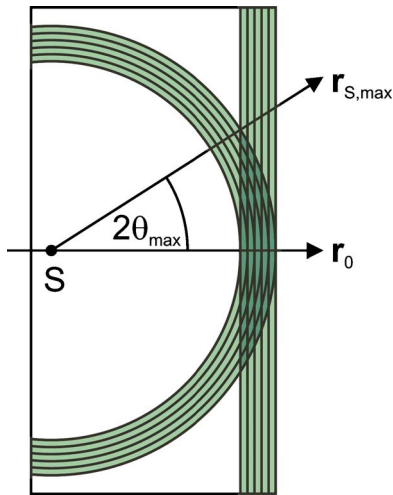


Fig. 6. (Color online) Schematic sketch of the overlap between a pulse, which propagates through the crystal in the direction \mathbf{r}_0 , and a spherical pulsed wave originating from its interaction with a scattering center \mathbf{S} close to the front of the crystal. The vector $\mathbf{r}_{S,\max}$ indicates the direction of wavefront propagation for scattered light with the largest angle $2\theta_{\max}$ towards \mathbf{r}_0 that still overlaps with the main pulse at the end of the crystal.

where, but only in a small paraboloidal region, the light scattered out of a pulse overlaps with the pulse itself. This overlap is necessary for the pulse and the scattered light to interfere and to write gratings and therefore is vital for the self-amplification process. Both wave packages should therefore overlap until the end of the crystal to get substantial amplification, and this obviously limits the possible angles of light-induced scattering with femtosecond pulses to $2\theta_{\max}$ and smaller. This leads to scattering of pulses mainly in the forward direction, which is what we observe. More precisely, the pulses must overlap coherently to interfere. Therefore, the relevant parameter is actually the coherence length rather than the pulse duration. However, since the pulses are nearly Fourier-transform-limited, both terms coincide in our case.

For the cw light used, the coherence length is several cm, which is larger than the dimensions of the crystals. Therefore, the scattering angles are not limited due to coherence: Here, light scattered under larger angles has a larger volume of the crystal available for self-amplification. In addition, larger grating vectors \mathbf{K} accompany larger scattering angles, which in turn favor a higher diffusion contribution and therefore a stronger beam coupling [21]. Both arguments lead to a higher efficiency of light diffraction at the grating and therefore to a stronger effect. Thus, for cw illumination, light-induced scattering under larger angles wins the competition.

This leads to the build-up of the light-climbing effect, as observed, if the geometrical conditions discussed in [20] are fulfilled. These conditions are equally satisfied for the fs pulse measurements, but the effect is obviously suppressed by the additional angular restrictions discussed above. Therefore, forward scattering processes dominate if LIS occurs for pulses. In our experiments with a focussed beam and in the measurements described in [14], the light-climbing effect is not possible even for cw light due to the small beam diameter, and thus the differ-

ence between the scattering of pulses and of cw light is much less pronounced or even absent.

C. Angular Selectivity

The different prevailing \mathbf{K} of scattering gratings for pulses and cw light can at least partially explain the different angular selectivities. A smaller \mathbf{K} for pulses means an effectively thinner grating, leading to a relaxed selectivity, and vice versa. In Fig. 4, lines are plotted according to a very simplified model based on the coupled wave theory [22], with the following assumptions:

- The incident light hits a single, homogeneous grating under the Bragg angle, where minimum transmission occurs.
- The scattering angle 2θ inside the crystal is assumed to be 28° for cw illumination (total internal reflection angle) and 6° for pulses, which is where we observe the maximum of scattered light.
- The strength of the grating is varied in order to fit it to the observed strength of η .

Considering, furthermore, a hologram thickness of 1/3 of the real crystal thickness, we get a reasonably good description of the experimental data (Fig. 4). This supports our basic idea that scattering into a smaller angular range relaxes the Bragg selectivity. However, for detailed modeling, the spread of the grating vectors has to be considered, as well as a correction of the effective thickness of the scattering holograms, because mostly the rear part of the crystal contributes. In addition, some bending of the holograms due to phase beam coupling may occur.

Phase beam coupling leads to a tilting of holographic gratings [23,24], which might explain the observed shift of the minimum of our angular selectivity curves. A detailed analysis of this effect is beyond the scope of this manuscript. For a deeper study, one has to consider in particular the intensity ratio between the pump wave and the scattered waves, since this influences the tilting direction of the grating. Depending on the assumptions, the explanation outlined above may predict two minima symmetrically located around the zero degree incidence angle, but such splitting has not been observed so far.

5. CONCLUSIONS

Light-induced scattering in $\text{LiNbO}_3:\text{Fe}$ shows different features for femtosecond pulses and cw illumination. Smaller scattering angles dominate for fs pulses, which can be explained by the short pulse duration and hence shorter coherence length for femtosecond pulses. In turn, the smaller deflection angles are the reason for a much broader angular selectivity of the light-induced scattering for pulsed illumination than for cw laser light. The shorter coherence length also explains that light-induced scattering of pulses is less pronounced in all investigated samples and even absent in $\text{LiNbO}_3:\text{Fe}$ with sufficiently low Fe^{2+} concentration. This is a remarkable, positive result, since $\text{LiNbO}_3:\text{Fe}$ crystals can be employed in applications with fs pulses without running into problems caused by light-induced scattering.

ACKNOWLEDGMENTS

We thank Lena Jentjens for the analysis of the interferometric data. Financial support from the Deutsche Forschungsgemeinschaft (DFG) Award BU 913/19-1 and from the Deutsche Telekom AG is gratefully acknowledged.

REFERENCES

1. R. Magnusson and T. K. Gaylord, "Laser scattering induced holograms in lithium niobate," *Appl. Opt.* **13**, 1545–1548 (1974).
2. S. G. Odoulov and M. S. Soskin, "Amplification, oscillation, and light-induced scattering in photorefractive crystals," in *Photorefractive Materials and Their Applications II*, 1st ed. (Springer-Verlag, 1989), Chap. 1, pp. 5–43.
3. G. Barbastathis, M. Balberg, and D. Brady, "Confocal microscopy with a volume holographic filter," *Opt. Lett.* **24**, 811–813 (1999).
4. W. Liu, D. Psaltis, and G. Barbastathis, "Real-time spectral imaging in three spatial dimensions," *Opt. Lett.* **27**, 854–856 (2002).
5. K. Buse, F. Havermeier, W. Liu, C. Moser, and D. Psaltis, "Holographic filters," in *Photorefractive Materials and Their Applications 3*, 2nd ed. (Springer Science+Business Media, LLC, 2007), Chap. 11, pp. 295–319.
6. P. Boffi, D. Piccinin, and M. C. Ubaldi, eds., *Infrared Holography for Optical Communications* (Springer-Verlag, 2003).
7. D. Z. Anderson, D. M. Lininger, and J. Feinberg, "Optical tracking novelty filter," *Opt. Lett.* **12**, 123–125 (1987).
8. M. Woerdemann, F. Holtmann, and C. Denz, "Full-field particle velocimetry with a photorefractive optical novelty filter," *Appl. Phys. Lett.* **93**, 021108 (2008).
9. P. Günter and J.-P. Huignard, eds., *Photorefractive Materials and Their Applications 3* (Springer Science+Business Media, LLC, 2007).
10. R. A. Rupp, "Material characterization by holographic methods," *Appl. Phys. A* **55**, 2–20 (1992).
11. M. Goulikov, M. Imlau, and T. Woike, "Photorefractive parameters of lithium niobate crystals from photoinduced light scattering," *Phys. Rev. B* **77**, 235110 (2008).
12. A. Ashkin, G. D. Boyd, J. M. Dziedzic, R. G. Smith, A. A. Ballman, J. J. Levinstein, and K. Nassau, "Optically-induced refractive index inhomogeneities in LiNbO₃ and LiTaO₃," *Appl. Phys. Lett.* **9**, 72–74 (1966).
13. R. A. Rupp, J. Marotz, K. H. Ringhofer, S. Treichel, S. Feng, and E. Krätzig, "Four-wave interaction phenomena contributing to holographic scattering in LiNbO₃ and LiTaO₃," *IEEE J. Quantum Electron.* **23**, 2136–2141 (1987).
14. Q. Wu, J. Xu, G. Zhang, L. Zhao, X. Zhang, H. Qiao, Q. Sun, W. Lu, G. Zhang, and T. Volk, "Fanning scattering in LiNbO₃ at 750–850 nm induced by femtosecond laser pulses," *Opt. Mater. (Amsterdam, Neth.)* **23**, 277–280 (2003).
15. G. Peterson, A. Glass, and T. Negran, "Control of susceptibility of lithium niobate to laser-induced refractive index changes," *Appl. Phys. Lett.* **19**, 130–132 (1971).
16. H. Kurz, E. Krätzig, W. Keune, H. Engelmann, U. Gonser, B. Dischler, and A. Räuber, "Photorefractive centers in LiNbO₃, studied by optical-, Mössbauer-, and EPR-methods," *Appl. Phys.* **12**, 355–368 (1977).
17. B. I. Sturman, S. G. Odoulov, and M. Y. Goulikov, "Parametric four-wave processes in photorefractive crystals," *Phys. Rep.* **275**, 197–254 (1996).
18. G. Zhang, N. Y. Kamber, J. Xu, S. Liu, Q. Sun, and G. Zhang, "Light-amplification competition between fanning noise and the signal beam in doped lithium niobate crystals," *J. Opt. Soc. Am. B* **16**, 905–910 (1999).
19. E. M. Avakyan, K. G. Belabaev, and S. G. Odoulov, "Polarized-anisotropy light-induced scattering in LiNbO₃:Fe crystals," *Fiz. Tverd. Tela (Leningrad)* **25**, 3274–3281 (1983).
20. S. Liu, J. Xu, G. Zhang, and Y. Wu, "Light-climbing effect in LiNbO₃:Fe crystal," *Appl. Opt.* **33**, 997–999 (1994).
21. N. V. Kukhtarev, V. B. Markov, S. G. Odoulov, M.-S. Soskin, and V. L. Vinetskii, "Holographic storage in electrooptic crystals. I: Steady-state," *Ferroelectrics* **22**, 949–960 (1979).
22. H. Kogelnik, "Coupled-wave theory for thick hologram gratings," *Bell Syst. Tech. J.* **48**, 2909–2947 (1969).
23. S. Tao, Z. H. Song, and D. R. Selviah, "Bragg-shift of holographic gratings in photorefractive Fe:LiNbO₃ crystals," *Opt. Commun.* **108**, 144–152 (1994).
24. K. Buse, S. Kämper, J. Frejlich, R. Pankrath, and K. H. Ringhofer, "Tilting of holograms in photorefractive Sr_{0.61}Ba_{0.39}Nb₂O₆ crystals by self-diffraction," *Opt. Lett.* **20**, 2249–2251 (1995).